

ChemComm

Accepted Manuscript



This is an *Accepted Manuscript*, which has been through the Royal Society of Chemistry peer review process and has been accepted for publication.

Accepted Manuscripts are published online shortly after acceptance, before technical editing, formatting and proof reading. Using this free service, authors can make their results available to the community, in citable form, before we publish the edited article. We will replace this *Accepted Manuscript* with the edited and formatted *Advance Article* as soon as it is available.

You can find more information about *Accepted Manuscripts* in the [Information for Authors](#).

Please note that technical editing may introduce minor changes to the text and/or graphics, which may alter content. The journal's standard [Terms & Conditions](#) and the [Ethical guidelines](#) still apply. In no event shall the Royal Society of Chemistry be held responsible for any errors or omissions in this *Accepted Manuscript* or any consequences arising from the use of any information it contains.

Cite this: DOI: 10.1039/c0xx00000x

www.rsc.org/xxxxxx

Communication

Ionic liquid-mediated synthesis of meso-scale porous lanthanum-transition-metal perovskites with high CO oxidation performance

Hanfeng Lu,^{a,b} * Pengfei Zhang,^b Zhen-an Qiao,^b Jinshui Zhang,^b Huiyuan Zhu,^b Jihua Chen,^c Yinfei Chen^a and Sheng Dai^{b,d,*}Received (in XXX, XXX) Xth XXXXXXXXX 20XX, Accepted Xth XXXXXXXXX 20XX
DOI: 10.1039/b000000x

Lanthanum-transition-metal perovskites with robust meso-scale porous frameworks (meso-LaMO₃) are synthesized through use of ionic liquids. The resultant samples demonstrate a rather high activity for CO oxidation, by taking advantage of unique nanostructure-derived benefits. This synthesis strategy opens up a new opportunity for preparing functional mesoporous complex oxides of various compositions.

Lanthanum transition metal perovskites (LaMO₃, M = Mn, Fe, Co, Ni) are highly attractive for many applications—including catalysis,¹ chemical sensors,² solid oxide fuel cells,³ and pseudocapacitors⁴—because of their unique physicochemical and electronic properties such as redox potential, ion mobility, semiconductive electronic structure, and rather high thermal stability.⁵ There are many well-established synthetic protocols for LaMO₃ preparation, for example, co-precipitation,⁶ citrate sol-gel,⁷ and mechanochemistry.⁸ However, the samples derived from such synthetic methods are bulk materials with relatively low surface areas (<10 m².g⁻¹), which greatly restricts their performance in target applications, particularly heterogeneous catalysis. The incorporation of mesopores in bulk LaMO₃ therefore is regarded as an ideal solution to address the above issue. Textural engineering of metal oxides with an accessible meso-scale porous framework would, in principle, not only facilitate mass transfer but also provide more catalytic sites for surface reactions.⁹ Toward this end, meso-scale porous LaMO₃ samples (meso-LaMO₃) with different morphologies have been successfully synthesized with the aid of sacrificial hard templates (for example, mesoporous silica).¹⁰ However, the removal of the hard templates often presents serious safety problems because it requires the use of toxic agents such as HF and NaOH.¹¹ In addition, the strong host-guest interaction induced by the crystallization of LaMO₃ perovskite at elevated temperatures often results in incomplete removal of parent templates, making the synthesis of template-free LaMO₃ difficult.¹² Hence it is highly desirable to develop an alternative synthetic strategy for meso-LaMO₃ fabrication.

Evaporation-induced self-assembly (EISA) was considered a highly efficient protocol for the synthesis of mesoporous metal oxides and their mixed oxides.¹³ However, organic surfactants used in EISA, such as CTAB (cetyl trimethylammonium

bromide) and P123 (tri-block copolymer), always decompose before they well crosslink with metal-containing species, owing to their low thermal stability. This instability issue associated with the current soft templates often results in an unstable mesoporous framework that easily collapses during crystallization of perovskite at elevated temperature.¹⁴ In this regard, an excellent thermal stable template with abundant anchoring sites for metal species coordination therefore is highly desirable for the construction of mesoporous LaMO₃ at elevated temperature. Recently, room temperature ionic liquids with rather high thermal stability have been extensively used as the porosity-directing agent for the preparation of carbon¹⁵, zeolites¹⁶, SiO₂¹⁷ and TiO₂¹⁸ based nanoarchitectures, greatly outstanding the development of nanochemistry.¹⁹ By taking of their supermolecule-like properties with rich hydrogen bonding networks, strong electrostatic interaction and good stability,²⁰ this kinds of ionic liquids chemically should also function as a promising media for the synthesis of meso-LaMO₃ perovskites.



Scheme. 1 The synthesis process for mesoporous lanthanum transition metal perovskite oxides by an ionic liquid

Herein, ionic liquids with good thermal stability against water and air were employed as soft media for nanostructural engineering of LaMO₃ perovskites with robust mesoporous frameworks via an enhanced electrostatic S⁺X⁻I⁺ self-assembly approach. In Scheme 1, lanthanum methoxyethoxide (LMEO) and a transition metal acetate were used as the precursors of lanthanum, and the transition metal (M) and the cation (S⁺) and anion (X⁻) of selected ionic liquids directly mediated the assembly of lanthanum and M inorganic species (I⁺). Lanthanum and M in nanodomains easily achieve the stoichiometric ligand of the

precursors. From the viewpoint of reaction dynamics, the stoichiometric ligand of the reaction reagents in nanodomains not only promotes the formation of LaMO_3 perovskites after heating but, more important, is beneficial for the construction of robust mesoporous frameworks. In addition, ionic liquids with molecular sizes ranging from 1 to 10 nm, should self-function as soft templates for meso-phase structure generation, making the pore size highly tunable. After being well aged in a high-temperature condition for further crosslinking, the ionic liquids can be extracted completely by acetonitrile and recycled in another new synthetic process (Fig. S1). The resultant nanocomposite film is further heated at elevated temperature to induce the formation of LaMO_3 perovskites. Experimentally, four kinds of LaMO_3 (M=Mn, Fe, Co, Ni) perovskites were mediated by the ionic liquid $[\text{Bmim}]^+\text{Tf}_2\text{N}^-$. See electronic supplementary information (ESI) for detailed synthetic procedures.

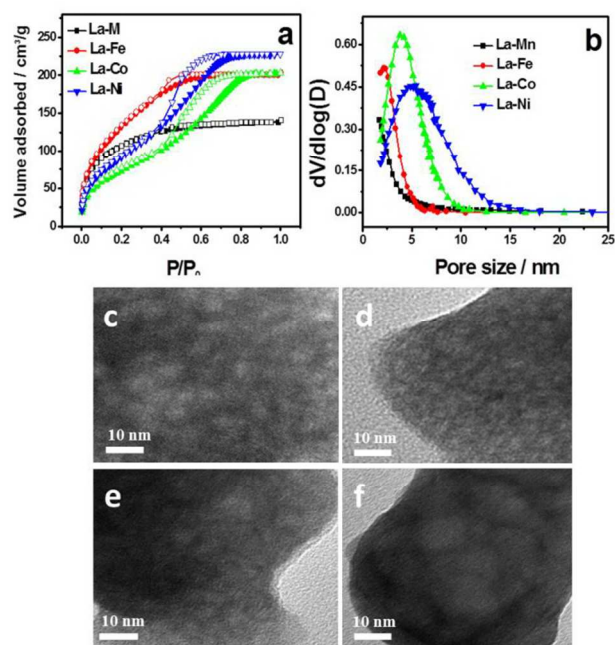


Fig.1 Characterization of as-made La-Mn, La-Fe, LaCo, and La-Ni nanocomposites by using the ionic liquid $[\text{Bmim}]^+\text{Tf}_2\text{N}^-$. (a) N_2 sorption isotherms of La-M nanocomposites; (b) BJH adsorption pore-size distributions of La-M nanocomposites; (c-f) TEM images of La-Mn, La-Fe, La-Co and La-Ni nanocomposite.

The textural structure of La-M (M=Mn, Fe, Co, Ni) nanocomposites after the complete extraction of ionic liquids was carefully examined by N_2 sorption and transmission electron microscopy (TEM). The surface areas of La-M (M=Mn, Fe, Co, Ni) derived from $[\text{Bmim}]^+\text{Tf}_2\text{N}^-$ media were determined to be 382, 505, 278 and 353 $\text{m}^2\cdot\text{g}^{-1}$, respectively, indicating that abundant nanopores were successfully incorporated in the lanthanum-M matrix (Table. S1). As expected, the N_2 -sorption isotherms and their corresponding Barrett-Joyner-Halenda (BJH) adsorption pore size distribution curves are closely dependent on the M species, owing to the difference in the electrostatic S^+XT^+ interaction (Fig. 1 a & b). For example, a transitional type of isotherm curve between typical I and IV curve was observed for La-Mn and La-Fe, corresponding to a pore size distribution at the microscale; whereas a representative type IV curve with an

evident capillary condensation step with a relative pressure of 0.5–0.8 was discovered for La-Co and La-Ni, corresponding to BJH pore sizes of 5 and 7 nm, respectively. In Fig. 1c-f, abundant wormlike nanopores in the La-M matrix are clearly imaged by TEM, in good agreement with the N_2 -sorption results.

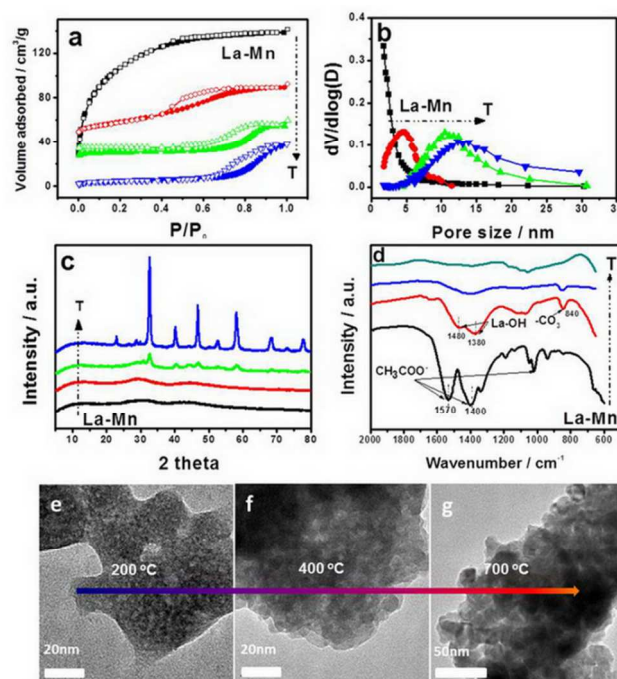


Fig.2 Characterization of La-Mn calcinated at different temperatures. (a) N_2 sorption isotherms of La-Mn (■) and La-Mn nanocomposites calcinated at 400 °C (●, shift up for 40 cm^3/g), 600 °C (▲, shift up for 20 cm^3/g); 700 °C (▼), (b) BJH adsorption pore-size distributions of La-Mn and calcined La-Mn; (c) XRD patterns of La-Mn and calcined La-Mn; (d) FTIR patterns of La-Mn and calcined La-Mn; (e-g) high-resolution TEM images of LaMnO_3 calcinated at 200, 400, and 700 °C.

The structural evolution of La-Mn nanocomposite under thermal treatment at different temperatures (400, 600, and 700 °C) was monitored by N_2 sorption isotherms, X-ray diffraction (XRD) patterns, Fourier-transform infrared (FTIR) spectra, and TEM images. When the heating temperature reached 400 °C, thermal decomposition of the inorganic species occurred (Fig. 2d), resulting in the significant transform of the N_2 -isotherm to a typical IV curve with an obvious H_2 -type hysteresis loop (Fig. 2a). Correspondingly, its BJH pore size increased from the microscale to 4 nm, clearly demonstrating the formation of mesopores in the La-Mn matrix (Fig. 2b). Further increasing the heating temperature to 600 °C induced the crystallization of LaMnO_3 perovskite (Fig. 2c), and a well-crystallized LaMnO_3 perovskite was obtained at 700 °C treatment (Fig. 2 c & d). The textural data (surface area and BJH pore size) for LaMnO_3 perovskite were determined to be 35 $\text{m}^2\cdot\text{g}^{-1}$ and 11 nm for the sample treated at 600 °C and 24 $\text{m}^2\cdot\text{g}^{-1}$ and 14 nm for the sample treated at 700 °C. The results indicate that mesoporous frameworks were indeed present in the LaMnO_3 perovskite matrix. The TEM images in Fig. 2 e-g display the porous evolution in the nanodomains, in which wormlike mesoporous structures with abundant cavities are clearly observed. Textural and crystallization information for other LaMO_3 (M=Fe, Co, Ni) perovskites treated at 650°C is provided in Fig S2. The surface

areas and BJH pore sizes of LaFeO₃, LaCoO₃, and LaNiO₃ were determined to be 20 m².g⁻¹ and 20 nm, 27 m².g⁻¹ and 8 nm, and 21 m².g⁻¹ and 9 nm, respectively (Table. S1).

As is well known, the self-assembly process containing metal organic salt is closely dependent on the amount of water added, which affects the initial hydrolysis and condensation of LMEO. Fig. S3 displays the N₂-sorption isotherms of La-Mn nanocomposites synthesized with different amounts of water in the precursor solution. It is interesting that microporous La-Mn nanocomposites with high surface areas of >350 m².g⁻¹ can be synthesized under H₂O/La (mol) in the wide range of 0 to 8, which means hydrolysis and self-assembly in this process do not require severe synthetic conditions (e.g., humidity, temperature, and pressure). Excessive hydrolysis occurs only when the ratio of H₂O to lanthanum is more than 12, which results in failure of self-assembly and a sharp decrease in surface area.

The other remarkable advantage of the ionic liquid-mediated synthetic approach is that by simply changing the cation (S⁺) molecule size of the ionic liquid, the pore structure of the La-M nanocomposites can also be easily adjusted. Taking the La-Mn nanocomposite as an example, as shown in the N₂-sorption isotherms and pore size distribution in Fig. S4, the La-Mn nanocomposites prepared by a protic [N_{8,8,8,H}]⁺Tf₂N⁻ ionic liquid all exhibit representative type IV curves with a sharp capillary condensation step in a relative pressure range of 0.7–0.9; these results indicate that larger pore sizes of 8–15 nm can be structured. More interesting, the La-M nanocomposites with larger pore sizes prepared by [N_{8,8,8,H}]⁺Tf₂N⁻ show a more robust meso-scale porous framework, the surface area of which can reach 36 m².g⁻¹ after heating at 700°C. We believe meso-LaMO₃ perovskites with higher surface areas could be synthesized using other potential ionic liquids.

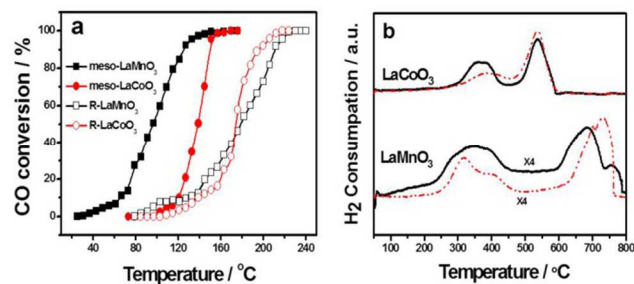


Fig.3 Characterization of activities and redox of meso-LaMnO₃, R-LaMnO₃, (calcinated at 700°C) and meso-LaCoO₃, R-LaCoO₃ (calcinated at 650 °C) perovskites. (a) Light-off curves of CO oxidation on mesoporous and bulk LaMnO₃ and LaCoO₃ (GHSV=20,000 mL (h gcat)⁻¹); (b) H₂-TPR curves of meso-LaMnO₃ and meso-LaCoO₃ (black solid lines), R-LaMnO₃ and R-LaCoO₃ (red dotted lines).

The enlarged surface areas of the meso-LaMO₃ perovskites make them promising candidates for application in heterogeneous catalysis. Catalytic oxidation of CO is a typical gas–solid reaction that has been extensively studied because of its applications in many fields,²¹ such as air purification, pollution control, and fuel cell technologies. Fig. 3a shows the catalytic performance toward CO oxidation of meso-LaMnO₃ and meso-LaCoO₃ perovskite samples prepared by [Bmim]⁺Tf₂N⁻. Performance data for bulk R-LaMnO₃ (7 m²/g) and R-LaCoO₃ (5 m²/g) prepared by the citrate sol-gel method are also included for comparison (the N₂ sorption

and XRD results of the samples see Fig. S5). Among these materials, meso-LaMnO₃ and meso-LaCoO₃ show extremely high activity, and CO can be completely oxidized at 130 °C on meso-LaMnO₃ and at 150 °C on meso-LaCoO₃. Their catalytic activity is much higher than that of R-LaMnO₃ and R-LaCoO₃, which exhibit 95% conversion at temperatures above 220 and 210°C, respectively. The meso-LaMnO₃ material was selected for long-term durability testing. The catalyst maintained 100% conversion, and no activity loss was observed for a consecutive 30 h at 140°C (Fig. S6).

The redox properties of meso-LaMnO₃ and meso-LaCoO₃ were investigated by H₂-TPR technology (Fig. 3b). Two reduction peaks were found at low temperatures (200–500°C) and at high temperatures (600–800°C) for all samples. The reaction peak areas of meso-LaMnO₃ and meso-LaCoO₃ at low temperatures were almost two fold higher than those of R-LaMnO₃ and R-LaCoO₃. For meso-LaMnO₃, in particular, the reduction temperature begins from 100 °C, which is quite consistent with the temperature of CO oxidation. In addition, the total H₂ consumption levels of mesoporous materials are higher than those of their corresponding bulk counterparts. This indicates that the pore structure and stoichiometric ligand assembly of lanthanum and transition metal not only dramatically promote redox performance by increasing the amount of active oxygen but also increase the ratio of transitional metal with a high valence, both of which are highly beneficial for heterogeneous catalytic oxidation reactions.

In summary, an ionic liquid-mediated synthetic strategy has been firmly established for the preparation of meso-LaMO₃ perovskites with robust crystalline frameworks. It takes advantage of the excellent thermal stability of ionic liquids to tightly crosslink the metal-containing species at high temperatures to construct a stable nanocomposition for nanotexture engineering. The high flexibility and compatibility of such synthetic strategies enable broad tunability of ionic liquids and metal precursors for the preparation of other kinds of perovskites. Benefiting from the pore structure and La-M ligand assembly, the resulting meso-LaMO₃ exhibits an extremely high activity and stability for CO oxidation. We believe the synthesis strategy reported here may open up new opportunities for preparing functional mesoporous complex mixed oxides of various compositions.

This work is supported by the U.S. Department of Energy, Office of Science, Basic Energy Sciences, Chemical Sciences, Geosciences, and Biosciences Division, the Natural Science Foundation of China (NO. 21107096), the Natural Science Foundation of Zhejiang province (NO.LY14E080008) and the Commission of Science and Technology of Zhejiang province (NO.2013C03021).

Notes and references

- ^a Institute of Catalytic Reaction Engineering, College of Chemical Engineering, Zhejiang University of Technology, Hangzhou, 310014, China, Fax: +86 0571 88320767; Tel: +86 0571 88320767; Email: luhf@zjut.edu.cn
- ^b Chemical Sciences Division, Oak Ridge National Laboratory, Oak Ridge, Tennessee 37831, United States, Email: dais@ornl.gov
- ^c Center for Nanophase Materials Sciences and Chemical Science Division, Oak Ridge National Laboratory

^d Department of Chemistry, University of Tennessee, Knoxville, Tennessee, 37996, United States

† Electronic Supplementary Information (ESI) available: Detailed description of the experimental procedure, characterization results. See DOI: 10.1039/b000000x/

- 1 (a) Y. Liu, H. Dai, J. Deng, L. Zhang, B. Gao, Y. Wang, X. Li, S. Xie and G. Guo, *Appl Catal B*, 2013, **140**, 317; (b) C. H. Kim, G. S. Qi, K. Dahlberg and W. Li, *Science*, 2010, **327**, 1624; (c) Y. Nishihata, J. Mizuki, T. Akao, H. Tanaka, M. Uenishi, M. Kimura, T. Okamoto and N. Hamada, *Nature*, 2002, **418**, 164; (d) S. Royer, D. Duprez, F. Can, X. Courtois, C. Batiot-Dupeyrat, S. Laassiri and H. Alamdari, *Chem Rev*, 2014, **114**, 10292.
- 15 2 (a) S. Pokhrel, L. H. Huo, H. Zhao and S. Gao, *Sens Actuators B*, 2007, **122**, 321; (b) M. M. Natile, A. Ponzoni, I. Concina and A. Glisenti, *Chem Mater*, 2014, **26**, 1505.
- 3 (a) L. M. Petkovic, V. Utgikar and S. N. Rashkeev, *J Phys Chem C*, 2011, **115**, 8709; (b) X. Chen and S. P. Jiang, *J Mater Chem A*, 2013, **1**, 4871; (c) A. A. Yaremchenko, V. V. Kharton, V. A. Kolotygin, M. V. Patrakeev, E. V. Tsipis and J. C. Waerenborgh, *J Power Sources*, 2014, **249**, 483.
- 4 J. T. Mefford, W. G. Hardin, S. Dai, K. P. Johnston and K. J. Stevenson, *Nat Mater*, 2014, **13**, 726.
- 25 5 M. A. Pena and J. L. G. Fierro, *Chem Rev*, 2001, **101**, 1981.
- 6 (a) S. H. Liang, T. G. Xu, F. Teng, R. L. Zong and Y. F. Zhu, *Appl Catal B*, 2010, **96**, 267; (b) J. A. Villoria, M. C. Alvarez-Galvan, S. M. Al-Zahrani, P. Palmisano, S. Specchia, V. Specchia, J. L. G. Fierro and R. M. Navarro, *Appl Catal B*, 2011, **105**, 276.
- 30 7 (a) F. Teng, W. Han, S. H. Liang, B. G. Gaugeu, R. L. Zong and Y. F. Zhu, *J Catal*, 2007, **250**, 1; (b) N. A. Merino, B. P. Barbero, P. Ruiz and L. E. Cadus, *J Catal*, 2006, **240**, 245.
- 8 (a) G. J. Zou, L. Chen and X. L. Wang, *Catal Lett*, 2009, **127**, 444; (b) Z. Sarshar, F. Kleitz and S. Kaliaguine, *Energy Environ Sci*, 2011, **4**, 4258.
- 35 9 (a) X. C. Wang, J. C. Yu, Y. D. Hou and X. Z. Fu, *Adv Mater*, 2005, **17**, 99; (b) T. Y. Ma, Y. Zheng, S. Dai, M. Jaroniec and S. Z. Qiao, *J Mater Chem A*, 2014, **2**, 8676.
- 10 (a) Y. X. Wang, X. Z. Cui, Y. S. Li, Z. Shu, H. R. Chen and J. L. Shi, *Microporous Mesoporous Mater*, 2013, **176**, 8; (b) M. M. Nair, F. Kleitz and S. Kaliaguine, *Chemcatchem*, 2012, **4**, 387; (c) Y. G. Wang, J. W. Ren, Y. Q. Wang, F. Y. Zhang, X. H. Liu, Y. Guo and G. Z. Lu, *J Phys Chem C*, 2008, **112**, 15293.
- 40 11 A.-H. Lu and F. Schueth, *Adv Mater*, 2006, **18**, 1793.
- 45 12 R. Zhang, P. Li, N. Liu, W. Yue and B. Chen, *J Mater Chem A*, 2014, **2**, 17329.
- 13 (a) C. J. Brinker, Y. F. Lu, A. Sellinger and H. Y. Fan, *Adv Mater*, 1999, **11**, 579; (b) A. S. Poyraz, C.-H. Kuo, S. Biswas, C. K. King'ondo and S. L. Suib, *Nat Commun*, 2013, **4**; (c) T. Brezesinski, M. Groenewolt, A. Gibaud, N. Pinna, M. Antonietti and B. M. Smarsly, *Adv Mater*, 2006, **18**, 2260.
- 50 14 R. Chao, R. Munprom, R. Petrova, K. Gerdes, J. R. Kitchin and P. A. Salvador, *J Am Ceram Soc*, 2012, **95**, 2339.
- 15 (a) Z. Y. Zhang, G. M. Veith, G. M. Brown, P. F. Fulvio, P. C. Hillesheim, S. Dai and S. H. Overbury, *Chem Commun*, 2014, **50**, 1469; (b) J. S. Lee, X. Q. Wang, H. M. Luo and S. Dai, *Adv Mater*, 2010, **22**, 1004; (c) X. Q. Wang and S. Dai, *Angew Chem Int Ed*, 2010, **49**, 6664.
- 60 16 E. R. Cooper, C. D. Andrews, P. S. Wheatley, P. B. Webb, P. Wormald and R. E. Morris, *Nature*, 2004, **430**, 1012.
- 17 (a) S. Dai, Y. H. Ju, H. J. Gao, J. S. Lin, S. J. Pennycook and C. E. Barnes, *Chem Commun*, 2000, 243; (b) B. G. Trewyn, C. M. Whitman and V. S. Y. Lin, *Nano Lett*, 2004, **4**, 2139; (c) Y. Zhou, J. H. Schattka and M. Antonietti, *Nano Lett*, 2004, **4**, 477.
- 65 18 (a) S. H. Zhou, Z. Ma, G. A. Baker, A. J. Rondinone, Q. Zhu, H. M. Luo, Z. L. Wu and S. Dai, *Langmuir*, 2009, **25**, 7229; (b) Y. Zhou and M. Antonietti, *J Am Chem Soc*, 2003, **125**, 14960.
- 19 (a) A. Taubert and Z. Li, *Dalton Trans*, 2007, 723; (b) Z. Ma, J. H. Yu and S. Dai, *Adv Mater*, 2010, **22**, 261; (c) M. Antonietti, D. B. Kuang, B. Smarsly and Z. Yong, *Angew Chem Int Ed*, 2004, **43**, 4988; (d) R. E. Morris, *Chem Commun*, 2009, 2990.
- 70 20 (a) Z. Hu and C. J. Margulis, *Acc Chem Res*, 2007, **40**, 1097; (b) Z. Hu and C. J. Margulis, *Proc Natl Acad Sci*, 2006, **103**, 831; (c) A. Mele, C. D. Tran and S. H. D. Lacerda, *Angew Chem Int Ed*, 2003, **42**, 4364.
- 75 21 (a) P. Venkataswamy, K. N. Rao, D. Jampaiah and B. M. Reddy, *Appl Catal B*, 2015, **162**, 122; (b) P. Xiao, J. Zhu, H. Li, W. Jiang, T. Wang, Y. Zhu, Y. Zhao and J. Li, *Chemcatchem*, 2014, **6**, 1774; (c) S. J. Huang, K. Hara and A. Fukuoka, *Energy Environ Sci*, 2009, **2**, 1060.